The Journal of Chemical Physics

# The effects of monovalent metal cations on the crystal and electronic structures of $Cs_2MBiCl_6$ (M = Ag, Cu, Na, K, Rb, and Cs) perovskites

Cite as: J. Chem. Phys. **153**, 141101 (2020); https://doi.org/10.1063/5.0021238
Submitted: 08 July 2020 . Accepted: 23 September 2020 . Published Online: 08 October 2020

Wenwu Shi, Tong Cai, Zhiguo Wang, and Ou Chen

The Journal of Chemical Physics COMMUNICATION scitation.org/journal/jcp

# The effects of monovalent metal cations on the crystal and electronic structures of $Cs_2MBiCl_6$ (M = Ag, Cu, Na, K, Rb, and Cs) perovskites

Cite as: J. Chem. Phys. 153, 141101 (2020); doi: 10.1063/5.0021238
Submitted: 8 July 2020 • Accepted: 23 September 2020 •
Published Online: 8 October 2020



Wenwu Shi,[1,2] Tong Cai,[2] Zhiguo Wang,[1,a)] and Ou Chen[2,a)]

## AFFILIATIONS

[1] University of Electronic Science and Technology of China, Chengdu 610054, People's Republic of China
[2] Department of Chemistry, Brown University, Providence, Rhode Island 02912, USA

**Note:** This paper is Part of the JCP Emerging Investigators Special Collection.
[a)] **Authors to whom correspondence should be addressed:** zgwang@uestc.edu.cn and ouchen@brown.edu

## ABSTRACT

Lead-halide perovskites have attracted much attention over the past decade, while two main issues, i.e., the lead-induced toxicity and materials' instability, limit their further practice in widespread applications. To overcome these limitations, an effective alternative is to design lead-free perovskite materials with the substitution of two divalent lead ions with a pair of monovalent and trivalent metal ions. However, fundamental physics and chemistry about how tuning material's composition affects the crystal phase, electronic band structures, and optoelectronic properties of the material have yet to be fully understood. In this work, we conducted a series of density functional theory calculations to explore the mechanism that how various monovalent metal ions influence the crystal and electronic structures of lead-free $Cs_2MBiCl_6$ perovskites. We found that the $Cs_2MBiCl_6$ (M = Ag, Cu, and Na) perovskites preferred a cubic double perovskite phase with low carrier effective masses, while the $Cs_2MBiCl_6$ (M = K, Rb, and Cs) perovskites favored a monoclinic phase with relatively high carrier effective masses. The different crystal phase preferences were attributed to the different radii of monovalent metal cations and the orbital hybridization between the metal and Cl ions. The calculation showed that all $Cs_2MBiCl_6$ perovskites studied here exhibited indirect bandgaps. Smaller bandgap energies for the perovskites with a cubic phase were calculated than those of the monoclinic phase counterparts. Charge density difference calculation and electron localization functional analysis were also conducted and revealed that the carrier mobility can be improved via changing the characteristics of metal-halide bonds through compositional and, thus, crystal structure tuning. Our study shown here sheds light on the future design and fabrication of various lead-free perovskite materials for optoelectronic applications.



## I. INTRODUCTION

Inorganic lead halide perovskites have been extensively studied over the last decade due to their unique optoelectronic properties.[1–10] Despite many of their superior merits, the toxicity induced by the involvement of the lead element and the instability of materials under ambient conditions are the two main obstacles for lead halide perovskites, largely hindering their real-world practice in widespread applications.[11–13] To this extent, developing lead-free perovskite materials represents a feasible and effective means to overcome these drawbacks.[2,12,14–19] One of the most promising strategies to access lead-free perovskites is to replace two $Pb^{2+}$ cations by a pair of monovalent [M(I)] and trivalent [M(III)] metal cations, resulting in the $Cs_2M(I)M(III)X_6$ perovskites including the "elpasolite" double perovskite (cubic phase) or the zero-dimensional (0D) perovskite structure (monoclinic phase) (Scheme 1).[20–26] Among this family of materials, Bi-based (i.e., $Cs_2MBiX_6$) perovskites have drawn a significant amount of attention

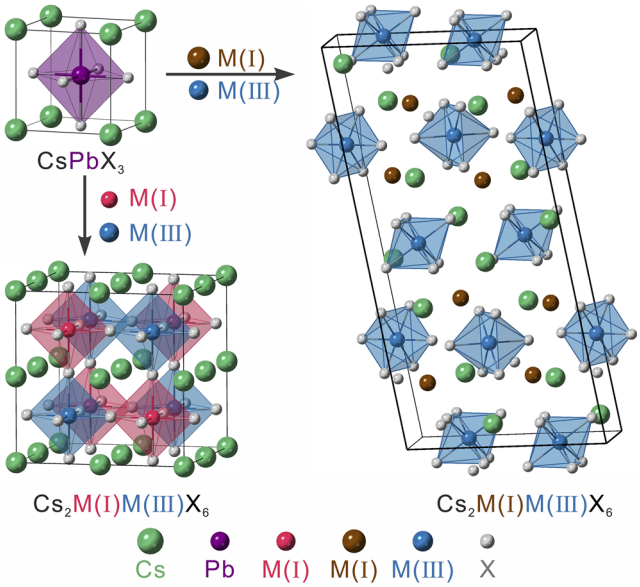


**SCHEME 1**. Schematics of metal halide perovskite crystal structures: 3D cubic perovskite $CsPbX_3$, lead-free $Cs_2M(I)M(III)Cl_6$ cubic double perovskites, and 0D $Cs_2M(I)M(III)Cl_6$ monoclinic perovskites.

owing to the enhanced materials' stability, unique electronic structures, and controllable bandgaps and photoluminescences.[22,26–28] Since the band structures of $Cs_2MBiX_6$ perovskites mainly originated from the $[MX_6]^{5-}$ and/or $[BiX_6]^{3-}$ octahedral units,[19,29–32] their electronic properties can be tailored by choosing a suitable combination of metal and halide compositions. Therefore, altering monovalent cation (i.e., $M^+$) in the $Cs_2MBiCl_6$ perovskites could lead to distinct crystal structures as well as optoelectronic characteristics. To date, various $Cs_2MBiCl_6$ materials at both nano- and bulk-scales have been successfully synthesized and studied. For example, $Cs_2AgBiCl_6$ nanocrystals with a cubic double perovskite phase were successful synthesized experimentally with an emission peak centered at 680 nm.[26] Feng *et al.* reported that the bulk $Cs_2CuBiCl_6$ also exhibited a cubic structure with a narrow indirect bandgap of 0.83 eV.[33] Theoretical calculations showed that $Cs_2NaBiCl_6$ cubic double perovskites possessed much wider bandgaps of 2.86 eV and 3.73 eV at room temperature depending on whether or not the spin–orbit coupling (SOC) effect is considered.[34,35] For the case of $Cs_2CsBiCl_6$ (i.e., $Cs_3BiCl_6$), a monoclinic crystal structure along with a wide indirect bandgap in the range of 3.73 eV–3.76 eV was observed.[18,29,36] Moreover, a crystal phase transition from cubic to triclinic was reported in the $Cs_{2-x}K_{x+1}BiCl_6$ solid solution when increasing the $K^+$ cation concentration at room temperature.[37] These studies showed different crystal and electronic structures for the $Cs_2MBiX_6$ perovskites with different monovalent metal ions ($M^+$).

To obtain a deeper understanding of this important category of materials, in this work, we have performed a series of density functional theory (DFT) calculations to study the crystal structures and electronic properties of $Cs_2MBiCl_6$ perovskites. Six different monovalent metal ions ($M^+$), i.e., $Ag^+$, $Cu^+$, $Na^+$, $K^+$, $Rb^+$, and $Cs^+$ were chosen as model systems. DFT calculation results show that the Ag-, Cu-, and Na-based perovskites possess a cubic double perovskite structure with small indirect bandgaps, whereas the K-, Rb-, and Cs-based systems exhibit a monoclinic structure with relatively large indirect bandgaps. These drastic differences in the crystal phase and electronic structures were attributed to various monovalent metal cation radii and orbital hybridization between the metal and Cl ions. These calculation results are consistent with our experimental data as well as previous reports.[18,26,27,29,38–41] The detailed understanding of series $Cs_2MBiCl_6$ perovskites shown in this work sheds light on the future design and fabrication of various lead-free perovskite materials in a predictable and controllable manner for applications.

## II. RESULTS AND DISCUSSION

Theoretical calculations were performed to explore the phase stability (cubic or monoclinic phase) at 0 K environment (Fig. 1, see the supplementary material for calculation details). Phase stability of $Cs_2MBiCl_6$ perovskites is evaluated by calculating the energy difference per atom ($\Delta E$) between the cubic and monoclinic phases using equation $\Delta E = E_{cubic} - E_{monoc}$, where $E_{cubic}$ and $E_{monoc}$ are the total energies of $Cs_2MBiCl_6$ perovskites per atom in cubic (space group: $Fm\bar{3}m$) and monoclinic (space group: $C2/c$) phases, respectively. It can be interpreted that the cubic (monoclinic) phase is the thermodynamically favored crystal phase when $\Delta E$ is negative (positive). Figure 1(b) shows the $\Delta E$ for $Cs_2MBiCl_6$ perovskites with six monovalent metal ions, i.e., $Ag^+$, $Cu^+$, $Na^+$, $K^+$, $Rb^+$, and $Cs^+$, all of which have been studied in experiments.[18,26,27,29,38–42] Among these elements, the $Ag^+$ and $Cu^+$ ions possess valence electrons in the frontier s- and d-orbitals, whereas the $Na^+$, $K^+$, $Rb^+$, and $Cs^+$ ions only have the valence electrons in s- and p-orbitals. The calculation results show that the $Cs_2MBiCl_6$ perovskites with M = Ag, Cu, and Na prefer the cubic double perovskite phase, while the $Cs_2MBiCl_6$ ones with M = K, Rb, and Cs favor the monoclinic phase [Fig. 1(b)]. This phase preference agrees well with previous reports as well as our experimental results (Fig. S1).[18,26,27,29,38–41] To gain details of the crystal structures, we further calculated the M–Cl bond length (BL) and different bond angles (BAs), as shown in Fig. 1(a), for the six perovskite systems [Figs. 1(a), 1(c), and 1(d)]. The calculation results show that the M–Cl BL is related to the radius ($r_M$) of the monovalent metal ions. Increasing the ionic size increased the respective calculated BLs from 2.74 Å for Ag, 2.55 Å for Cu, 2.79 Å for Na, 3.46 Å for K, and 3.57 Å for Rb to 3.63 Å for Cs [Fig. 1(c)]. The evolutions of BAs including Bi–Cl–M ($\theta_{BCM}$), Cl–Bi–Cl ($\theta_{CBC}$), and Cl–M–Cl ($\theta_{CMC}$) are shown in Fig. 1(d). All three BAs were determined to be 180° for the cases of M = Ag, Cu, and Na, indicating good preservation of the cubic double perovskite crystal phase [Fig. 1(d)]. However, these BAs were calculated to be in the ranges of 141°–143° for $\theta_{BCM}$, 177.57°–177.78° for $\theta_{CBC}$, and 142.59°–142.81° for $\theta_{CMC}$ for the cases of M = K, Rb, and Cs [Fig. 1(d)], indicating the structural deviation from a cubic structure to a distorted monoclinic structure [Fig. 1(a)]. Slightly enlarged deviation from the cubic phase as increasing the ionic radius revealed an ionic size-dependent distortion of octahedral units.[37,43,44]

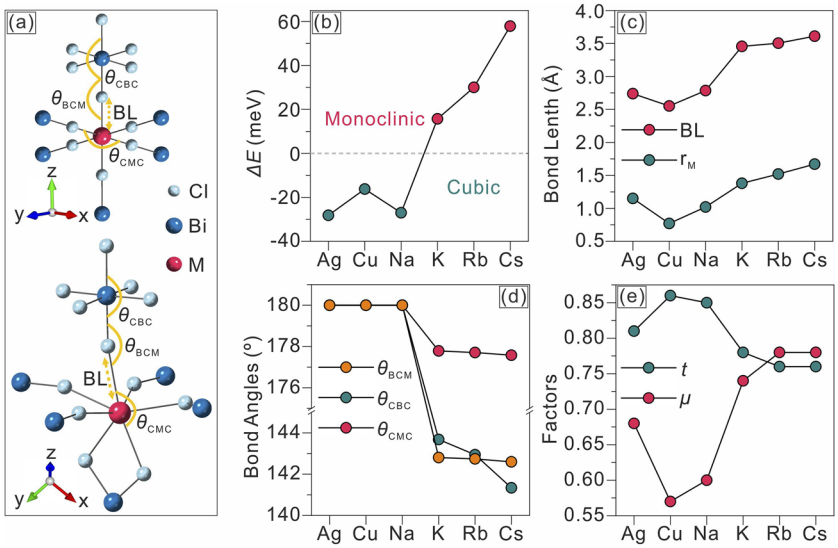


**FIG. 1.** General parameters of $Cs_2MBiCl_6$ perovskites with different M compositions (M = Ag, Cu, Na, K, Rb, and Cs). (a) Schematics to show the bond length (BL) and bond angles (BAs) of $Cs_2MBiCl_6$ perovskites in cubic (top) and monoclinic (bottom) phases. (b) Structural stability determination by energy difference ($\Delta E$). (c) The BL and radius of the monovalent metal ions ($r_M$), (d) BAs, and (e) the tolerance factor ($t$) and octahedral factor ($\mu$) for different $Cs_2MBiCl_6$ perovskites studied here.

Goldschmidt's empirical principle using the octahedral factor ($\mu$) and the Goldschmidt tolerance factor ($t$) has been commonly applied to evaluate the crystal phase stability of perovskites.[45–47] In order to maintain a stable octahedral structure, thus the cubic perovskite phase (space group: $Fm\bar{3}m$), the octahedral factor ($\mu$) needs to be between 0.442 and 0.895, while the tolerance factor ($t$) is required to be between 0.80 and 1.10.[45] The calculated $\mu$ and $t$ values for all the six types of $Cs_2MBiCl_6$ perovskites are shown in Fig. 1(e). While all the $\mu$ values are calculated to be between 0.57 and 0.78, within the predicted range for stabilizing perfect octahedral structures, the obtained $t$ values spread in and out of the required tolerance factor range [Fig. 1(e)]. Specifically, the $t$ values of 0.78, 0.76, and 0.76, respectively, for $Cs_2KBiCl_6$, $Cs_2RbBiCl_6$, and $Cs_2CsBiCl_6$ perovskites are all below the lower threshold value of 0.80, indicating their tendency of crystallizing into distorted perovskite structures (e.g., the monoclinic phase), as observed experimentally (Fig. S1).[18,29,37,48]

The correlation between the electronic band edge configurations and the $[MX_6]^{5-}$ octahedral units has been reported,[19,29] which inspired us to further conduct the calculations of the band structure and density of states (DOS) for the $Cs_2MBiCl_6$ perovskites. The SOC effect is taken into consideration in our calculations due to the splitting of $6p_{1/2}$ and $6p_{3/2}$ states of Bi in the conduction band.[49,50] For comparison, the corresponding band structure calculations using only the Perdew–Burke–Ernzerhof (PBE) functional without considering the SOC effect were also performed and shown in Fig. S2. With or without the consideration of SOC, the features of the valence band edge are almost unchanged (Figs. 2 and S2). In contrast, due to the strong SOC effects, the conduction band edge splits into two bands with separation energy larger than 0.39 eV at the L point after taking the SOC effect into consideration (Fig. 2). Thus, the obtained bandgaps are reduced, and the shapes of the conduction band are drastically changed (Fig. 2). This result is somewhat expected, given that the character of the conduction band edge is predominantly determined by the Bi-6$p$ orbitals. Therefore, the inclusion of the SOC effects is needed for correct descriptions of band structures and effective masses of the $Cs_2MBiCl_6$ perovskites.

The calculation results show that the band structure and projected DOS (PDOS) of $Cs_2AgBiCl_6$ perovskites exhibited semiconductor characteristics with an indirect bandgap of 1.54 eV [Fig. 2(a)].[49] The calculated conduction band minimum (CBM) and valence band maximum (VBM) were located at the L and X points in its first Brillouin zone, respectively [Fig. 2(a)]. The CBM originates mainly from the Cl-3$p$, Bi-6$p$ and Ag-5$s$ orbitals with a small contribution from the Ag-4$d$ orbital. In contrast, the VBM is mainly composed of the Ag-4$d$ and Cl-3$p$ orbitals with a minimum contribution from Bi-6$s$ orbitals [Fig. 2(a)]. Comparing to the Ag-containing case, the $Cs_2CuBiCl_6$ possesses a much smaller indirect bandgap of 0.68 eV with the CBM lying at the Γ symmetry point and the VBM lying at the X point [Fig. 2(b)]. The PDOS calculation shows that the CBM mainly consists of Cl-3$p$, Bi-6$p$, Cu-4$s$, and Cu-3$d$ orbitals, while Cu-3$d$, Cl-3$p$ orbitals and Bi-6$s$ orbitals are the major components for VBM [Fig. 2(b)]. Although having the same cubic double perovskite phase, a much larger indirect bandgap energy (2.98 eV) for the $Cs_2NaBiCl_6$ perovskite than those of $Cs_2AgBiCl_6$ (1.54 eV) and $Cs_2CuBiCl_6$ (0.68 eV) perovskites was obtained [Fig. 2(c)]. Unlike the Ag- and Cu-containing cases where strong orbital hybridizations occur between the frontier $s$, $d$ orbitals of the transition metals (i.e., Ag-5$s$, Ag-4$d$, and Cu-4$s$, Cu-3$d$), and Bi-6$p$, Cl-3$p$ orbitals, the absence of $d$-orbitals for Na atom results in drastically reduced orbital interactions, thus minimizing the Na-contribution to the CBM. Consequently, the CBM energy is raised, leading to a lager bandgap energy of 2.98 eV [Fig. 2(c)]. Band structures and PDOS were also calculated for $Cs_2MBiCl_6$ (M = K, Rb, and Cs) perovskites [Figs. 2(d)–2(f)]. For all these cases, the CBMs are positioned at the Γ symmetry point and the VBMs are located between A and B points [Figs. 2(d)–2(f)]. Similar to the $Cs_2NaBiCl_6$ perovskite, weak orbital interactions between M and Bi/Cl ions lead to minimal contributions from these alkali metal ions to CBMs, resulting in wide bandgap energies of

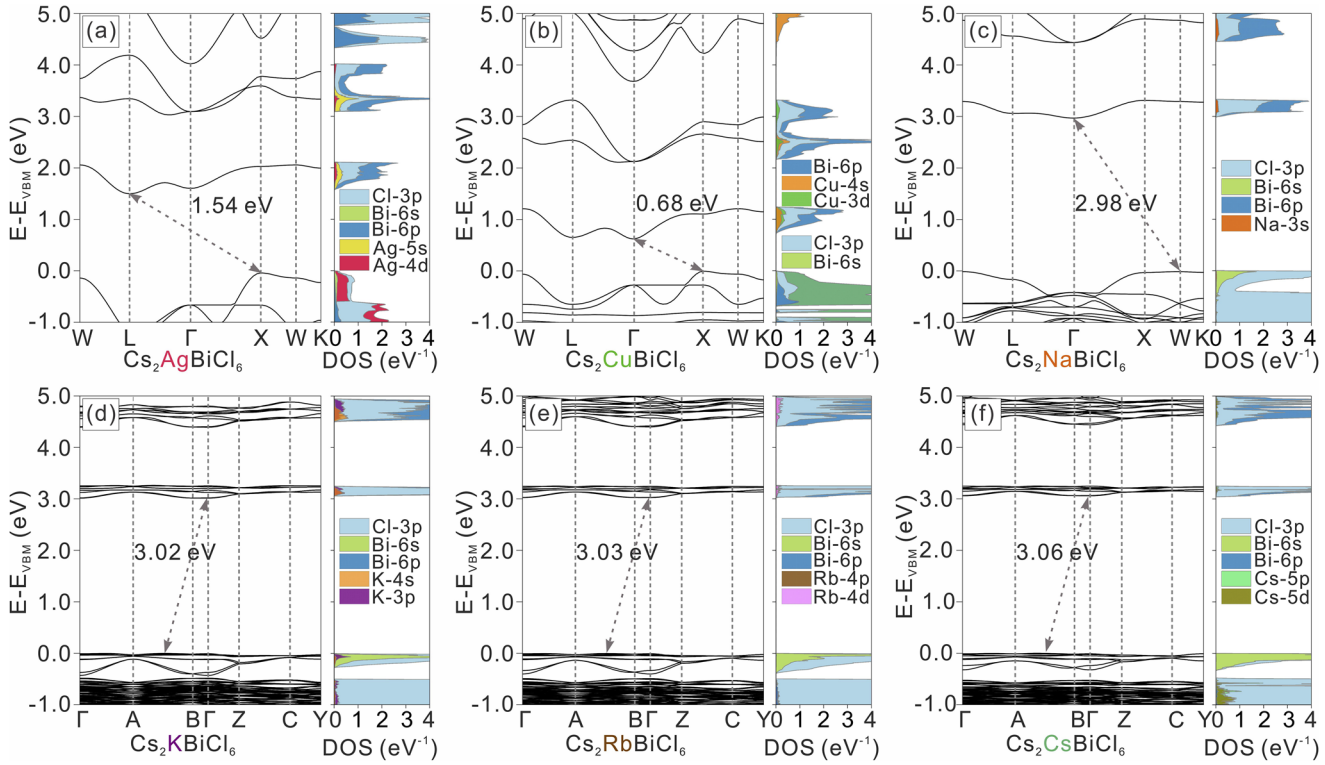


**FIG. 2**. Band structures and projected density of states (PDOS) calculations for $Cs_2MBiCl_6$ perovskites using the PBE + SOC functional. (a) $Cs_2AgBiCl_6$, (b) $Cs_2CuBiCl_6$, and (c) $Cs_2NaBiCl_6$ are in the cubic phase. (d) $Cs_2KBiCl_6$, (e) $Cs_2RbBiCl_6$, and (f) $Cs_2CsBiCl_6$ are in the monoclinic phase. The CBM and VBM are marked by dashed line arrows and the VBM energy is set to zero.

3.02 eV, 3.03 eV, and 3.06 eV for M = K, Rb, and Cs, respectively [Figs. 2(d)–2(f)]. These PDOS calculation results are compliant with the experimentally measured absorption peaks at 3.56 eV and 3.64 eV, respectively, for the $Cs_2CsBiCl_6$ ($Cs_3BiCl_6$) and $Cs_2NaBiCl_6$ perovskites (Fig. S1), which can be solely assigned to the electronic transition of $^1S_0 \rightarrow {}^3P_1$ for the $[BiCl_6]^{3-}$ units.[18,51–53]

Owing to its direct correlation with the photocarrier mobility, a crucial optoelectronic property of perovskite materials, we further investigated the carrier effective mass ($m^*$) at the band edge of the $Cs_2MBiCl_6$ perovskites (Table I). The equation, $m^* = \hbar\left[\frac{d^2E(k)}{dk^2}\right]^{-1}$, was employed for the calculation,[54] where $m^*$ is the effective mass, $\hbar$ is the reduced Planck's constant, $E(k)$ is the eigenvalue, and $k$ is the wave vector. Low carrier effective masses for both electron and hole were obtained at the band edges, respectively, along the L–W and X–Γ directions for the $Cs_2AgBiCl_6$ double perovskite ($m_e^* = 0.46m_0$ and $m_h^* = 0.23m_0$, where $m_0$ is the free electron mass) and along Γ–L and X–Γ directions for $Cs_2CuBiCl_6$ double perovskites

**TABLE I**. Calculated effective masses of $Cs_2MBiCl_6$ perovskites. $m_e{}^*$ and $m_h{}^*$ are the effective masses of electron and hole in the free electron mass $m_0$ unit. The L, W, Γ, X, A, Z, and B are the high-system points in the first Brillouin zone. The Λ symbol indicates the VBM point (between A and B) for $Cs_2MBiCl_6$ (M = K, Rb, and Cs). The symbol in the brackets shows the directions along which the effective masses were obtained.

| System | $m_e^*$ (direction) | $m_e^*$ (direction) | $m_h^*$ (direction) | $m_h^*$ (direction) |
|---|---|---|---|---|
| $Cs_2AgBiCl_6$ | 0.46 (L–W) | 0.69 (L–Γ) | 0.23 (X–Γ) | 0.90 (X–W) |
| $Cs_2CuBiCl_6$ | 0.39 (Γ–L) | 0.40 (Γ–X) | 0.26 (X–Γ) | 1.17 (X–W) |
| $Cs_2NaBiCl_6$ | 0.97 (Γ–L) | 1.80 (Γ–X) | 3.38 (W–X) | 6.30 (W–K) |
| $Cs_2KBiCl_6$ | — (Γ–B) | 1.09 (Γ–Z) | 4.38 (Λ–A) | 4.38 (Λ–B) |
| $Cs_2RbBiCl_6$ | — (Γ–B) | 1.09 (Γ–Z) | 5.88 (Λ–A) | 10.10 (Λ–B) |
| $Cs_2CsBiCl_6$ | — (Γ–B) | 1.09 (Γ–Z) | 4.81 (Λ–A) | 48.07 (Λ–B) |

($m_e^* = 0.39m_0$ and $m_h^* = 0.26m_0$) (Table I). Noticeably higher effective hole mass ($m_e^* = 0.97m_0$ and $m_h^* = 3.38m_0$) was obtained for the $Cs_2NaBiCl_6$ double perovskite (Table I), indicating unbalanced carrier mobilities for the material. For the cases of M = K, Rb, and Cs, both the electron and hole effective masses were calculated to be higher than those of the ones for cubic double perovskite cases (i.e., M = Ag, Cu, and Na) (Table I). These calculation results reveal that the cubic double perovskites studied here show relatively lower carrier effective masses, thus higher carrier mobilities than those with a monoclinic crystal phase (i.e., M = K, Rb, and Cs), in accordance with the isolation of octahedral units inside the monoclinic crystal lattices (Scheme 1).

Charge transfer and separation for the $Cs_2MBiCl_6$ perovskites were investigated by calculating the charge density difference $\Delta\rho(r)$ following the equation $\Delta\rho(r) = \rho_{comp} - \rho_{Cs} - \rho_M - \rho_{Bi} - \rho_{Cl}$, where $\rho_{comp}$, $\rho_{Cs}$, $\rho_M$, $\rho_{Bi}$, and $\rho_{Cl}$ are the charge densities of the $Cs_2MBiCl_6$ compound and $Cs^+$, $M^+$, $Bi^{3+}$, and $Cl^-$ are ions in the $Cs_2MBiCl_6$ perovskite crystal, respectively. The charge density differences are depicted in Figs. 3(a)–3(f), where the cyan and yellow regions correspondingly represent charge depletion and charge accumulation. It is clearly showed that the charge redistribution mainly occurred within the $[MCl_6]^{5-}$ octahedral units, where less charge losses were observed for M = Ag and Cu cases than the other four cases [Figs. 3(a)–3(f)]. The charge transfer was further quantified by the Bader charge population method.[55] The charge accumulation was kept as a nearly constant value, independent of the monovalent metal M variation (Fig. S3). When M (Ag, Cu, Na, K, Rb, and Cs) cation's radius increases, the charge loss also increases from 0.6*e* to 0.8*e*, while the charge loss number of Bi atoms keeps as a constant value of ~−1.5*e* (Fig. S3). The charge transfer can affect the bond characters between the M and Cl atoms, which can be further exhibited by calculating the electron localization functional (ELF) of the systems.

ELF has been proposed based on the second-order Taylor expansion of the spherically averaged pair density.[56] The ELF can be directly applied to visualize atomic shell structures, the distribution of the bonding and electron lone pairs in molecules, and to monitor changes in the electron distribution in bond-forming and bond-breaking processes.[57,58] To explore these electronic properties in our systems, ELF calculations have been conducted and the results

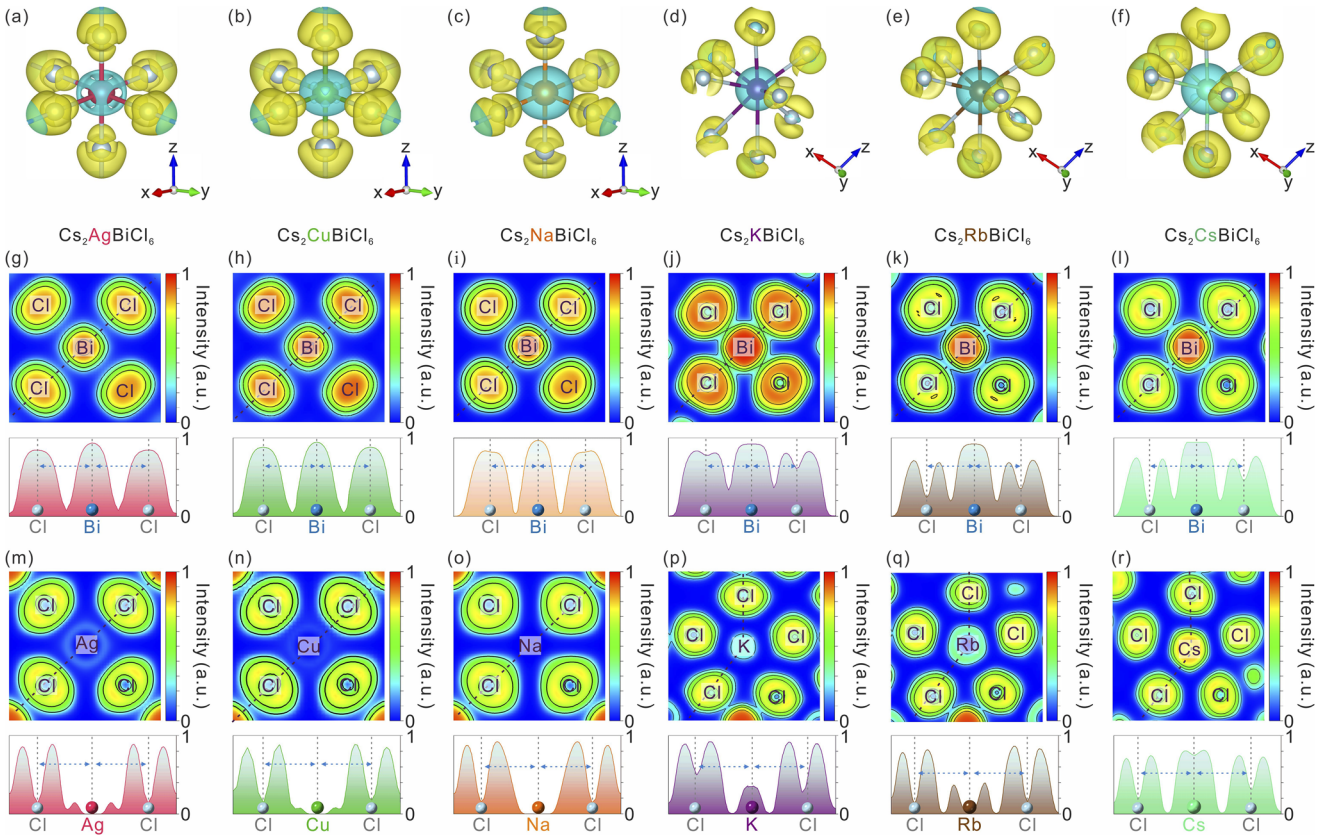


**FIG. 3**. Charge density difference calculation and electron localization functional (ELF) analysis. [(a)–(f)] The charge density difference (0.0045 e/bohr3) and [(g)–(r)] ELF of $Cs_2MBiCl_6$ perovskites. In [(a)–(f)], yellow surfaces correspond to the charge gains and cyan surfaces correspond to an equivalent charge loss. In [(g)–(r)], top panels display the associated ELF 2D mapping with color coding to represent the strength of electron density. Bottom panels show the 1D intensity profiles along the black dashed lines in the corresponding top panels, illustrating the electron density between different ions for $[BiCl_6]^{3-}$ [(g)–(l)] and $[MCl_6]^{5-}$ [(m)–(r)] octahedral units.

are shown in Figs. 3(g)–3(r). The ELF calculations clearly show the bond characteristics between metal cations (*i.e.*, $Cs^+$, $M^+$, and $Bi^{3+}$) and $Cl^-$ anions. For the $Cs_2MBiCl_6$ cubic double perovskite group (M = Ag, Cu, and Na), both the 2D mapping [Figs. 3(g)–3(i)], top panels) and the corresponding 1D intensity profiles [Figs. 3(g)–3(i)], bottom panels) show nearly no electron distribution (ELF value of ~0) in between any $Bi^{3+}$ and $Cl^-$ ion centers [Figs. 3(g)–3(i)]; the specific values of ELF between metal cations and $Cl^-$ anions are listed in Table S1 in the supplementary material. The absence of electron distribution unambiguously proved an ionic bond nature of the Bi–Cl bonds in these cases, consistent with the charge density calculation results [Figs. 3(a)–3(c)]. With the radius increasing from $Cu^+$ (77 pm) to $Ag^+$ (115 pm) ions, the ELF shows a decreased electron density near the $M^+$ cations from 0.067 to 0.055, indicating weak interactions between the $M^+$ and $Cl^-$ ions [Figs. 3(m)–3(o)]. However, the increased electron localization (ELF value of ~0) between the $Bi^{3+}$ cation and $Cl^-$ anion can be clearly visualized for the cases of $Cs_2MBiCl_6$ monoclinic perovskites (M = K, Rb, and Cs) [Figs. 3(j)–3(l)]. This electron sharing behavior between two ion centers indicates a more covalent bond characteristic of the Bi–Cl bonds in these cases [Figs. 3(j)–3(l)], Table S1). In addition, separate charge density accumulations near the $M^+$ and $Cl^-$ ions suggest the formation of stronger ionic bonds between the $M^+$ cations ($K^+$, $Rb^+$, and $Cs^+$) and $Cl^-$ anions as compared with cubic phase ones [Figs. 3(m)–3(r)]. The strong interactions between the cations ($Bi^{3+}$ and $M^+$) and $Cl^-$ ions in the $Cs_2MBiCl_6$ (M = K, Rb, and Cs) with a monoclinic phase result in large hole effective masses and the strong electronic localization effect at the VBM, which can be clearly visualized as a narrow orbital contribution band (from Bi-6*s* and Cl-3*p*) at the valence band edge in the PDOS plot [Figs. 2(d)–2(f)]. Due to this strong electron localization effect, electrons are mostly populated near the Bi and Cl atoms [Figs. 2(d)–2(f)]. The consequent high electronic binding energies of the $Cs_2MBiCl_6$ (M = K, Rb, and Cs) perovskites lead to a high energy electronic transition and a large energy gap between the valence and conduction bands. Furthermore, the enhanced interactions between the $Bi^{3+}$ and $Cl^-$ ions in the K-, Rb-, and Cs-containing $Cs_2MBiCl_6$ perovskites lead to distorted $[MCl_6]^{5-}$ octahedral units. As a result, the total system energies of the K-, Rb-, and Cs-containing $Cs_2MBiCl_6$ monoclinic perovskites are lower than the energies of their cubic double perovskite counterparts, leading to the monoclinic phase as the thermodynamic one (Figs. 1(b) and 2).

## III. CONCLUSIONS

In conclusion, we compared crystal structures and electronic properties of lead-free $Cs_2MBiCl_6$ perovskites with various M metal elements using DFT calculations. The results show that the $Cs_2MBiCl_6$ (M = Ag, Cu, and Na) perovskites possess a cubic double perovskite crystal phase with relatively low carrier effective masses and smaller bandgaps. In contrast, the $Cs_2MBiCl_6$ (M = K, Rb, and Cs) perovskites favor a monoclinic crystal phase with much higher carrier effective masses and larger bandgaps. The charge density difference calculation and ELF analyses show the composition induced different metal-halide bond features for the $Cs_2MBiCl_6$ perovskites with different crystal structures. We attribute the crystal phase preferences to different radii of monovalent metal (M) cations as well as the orbital hybridization between metal (M) and Cl ions. We anticipate that our study presented here can further advance the understanding of relationships between stoichiometry, crystal structure, and electronic properties of lead-free $Cs_2MBiCl_6$ perovskites that are of great importance for a wide range of optoelectronic applications.

## SUPPLEMENTARY MATERIAL

See the supplementary material for the complete experimental and calculation details including procedures, analyses, and band structures of PBE images.

## AUTHORS' CONTRIBUTIONS

W.S. and T.C. are contributed equally

## ACKNOWLEDGMENTS

O.C. acknowledges support from the Brown University startup fund. The computational parts of this research were conducted using computational resources and services at the Brown University Center for Computation and Visualization (CCV).

The authors declare no conflict of interest.

## DATA AVAILABILITY

The data that support the findings of this study are available from the corresponding author upon reasonable request.

## REFERENCES

[1] Q. A. Akkerman, G. Rainò, M. V. Kovalenko, and L. Manna, Nat. Mater. **17**, 394 (2018).
[2] J. Shamsi, A. S. Urban, M. Imran, L. De Trizio, and L. Manna, Chem. Rev. **119**, 3296 (2019).
[3] J. Huang, M. Lai, J. Lin, and P. Yang, Adv. Mater. **30**, 1802856 (2018).
[4] H. Yang, Y. Zhang, K. Hills-Kimball, Y. Zhou, and O. Chen, Sustainable Energy Fuels **2**, 2381 (2018).
[5] A. Swarnkar, V. K. Ravi, and A. Nag, ACS Energy Lett. **2**, 1089 (2017).
[6] J. De Roo, M. Ibáñez, P. Geiregat, G. Nedelcu, W. Walravens, J. Maes, J. C. Martins, I. Van Driessche, M. V. Kovalenko, and Z. Hens, ACS Nano **10**, 2071 (2016).
[7] K. Hills-Kimball, M. J. Pérez, Y. Nagaoka, T. Cai, H. Yang, A. H. Davis, W. Zheng, and O. Chen, Chem. Mater. **32**, 2489 (2020).
[8] M. Liu, M. B. Johnston, and H. J. Snaith, Nature **501**, 395 (2013).
[9] M. Que, Z. Dai, H. Yang, H. Zhu, Y. Zong, W. Que, N. P. Padture, Y. Zhou, and O. Chen, ACS Energy Lett. **4**, 1970 (2019).
[10] T. Cai, H. Yang, K. Hills-Kimball, J.-P. Song, H. Zhu, E. Hofman, W. Zheng, B. M. Rubenstein, and O. Chen, J. Phys. Chem. Lett. **9**, 7079 (2018).
[11] F. Giustino and H. J. Snaith, ACS Energy Lett. **1**, 1233 (2016).
[12] P. V. Kamat, J. Bisquert, and J. Buriak, ACS Energy Lett. **2**, 904 (2017).
[13] Q. Fan, G. V. Biesold-McGee, J. Ma, Q. Xu, S. Pan, J. Peng, and Z. Lin, Angew. Chem., Int. Ed. **59**, 1030 (2020).
[14] J. Sun, J. Yang, J. I. Lee, J. H. Cho, and M. S. Kang, J. Phys. Chem. Lett. **9**, 1573 (2018).
[15] B. Yang and K. Han, Acc. Chem. Res. **52**, 3188 (2019).

[16]B. Yang, X. Mao, F. Hong, W. Meng, Y. Tang, X. Xia, S. Yang, W. Deng, and K. Han, J. Am. Chem. Soc. **140**, 17001 (2018).
[17]T. Cai, W. Shi, S. Hwang, K. Kobbekaduwa, Y. Nagaoka, H. Yang, K. Hills-Kimball, H. Zhu, J. Wang, Z. Wang, Y. Liu, D. Su, J. Gao, and O. Chen, J. Am. Chem. Soc. **142**, 11927 (2020).
[18]H. Yang, T. Cai, E. Liu, K. Hills-Kimball, J. Gao, and O. Chen, Nano Res. **13**, 282 (2020).
[19]L. Zhang, K. Wang, and B. Zou, ChemSusChem **12**, 1612 (2019).
[20]F. Locardi, E. Sartori, J. Buha, J. Zito, M. Prato, V. Pinchetti, M. L. Zaffalon, M. Ferretti, S. Brovelli, I. Infante, L. De Trizio, and L. Manna, ACS Energy Lett. **4**, 1976 (2019).
[21]L. Schade, A. D. Wright, R. D. Johnson, M. Dollmann, B. Wenger, P. K. Nayak, D. Prabhakaran, L. M. Herz, R. Nicholas, H. J. Snaith *et al.*, ACS Energy Lett. **4**, 299 (2018).
[22]K.-z. Du, W. Meng, X. Wang, Y. Yan, and D. B. Mitzi, Angew. Chem., Int. Ed. **56**, 8158 (2017).
[23]B. Yang, J. Chen, S. Yang, F. Hong, L. Sun, P. Han, T. Pullerits, W. Deng, and K. Han, Angew. Chem., Int. Ed. **130**, 5457 (2018).
[24]B. Yang, F. Hong, J. Chen, Y. Tang, L. Yang, Y. Sang, X. Xia, J. Guo, H. He, S. Yang, W. Deng, and K. Han, Angew. Chem., Int. Ed. **131**, 2300 (2019).
[25]J. C. Dahl, W. T. Osowiecki, Y. Cai, J. K. Swabeck, Y. Bekenstein, M. Asta, E. M. Chan, and A. P. Alivisatos, Chem. Mater. **31**, 3134 (2019).
[26]N. Chen, T. Cai, W. Li, K. Hills-Kimball, H. Yang, M. Que, Y. Nagaoka, Z. Liu, D. Yang, A. Dong, C.-Y. Xu, R. Zia, and O. Chen, ACS Appl. Mater. Interfaces **11**, 16855 (2019).
[27]L. Zhang, Y. Fang, L. Sui, J. Yan, K. Wang, K. Yuan, W. L. Mao, and B. Zou, ACS Energy Lett. **4**, 2975 (2019).
[28]C. Wu, Q. Zhang, Y. Liu, W. Luo, X. Guo, Z. Huang, H. Ting, W. Sun, X. Zhong, S. Wei, S. Wang, Z. Chen, and L. Xiao, Adv. Sci. **5**, 1700759 (2018).
[29]S. E. Creutz, H. Liu, M. E. Kaiser, X. Li, and D. R. Gamelin, Chem. Mater. **31**, 4685 (2019).
[30]A. H. Slavney, T. Hu, A. M. Lindenberg, and H. I. Karunadasa, J. Am. Chem. Soc. **138**, 2138 (2016).
[31]M. K. Jana, S. M. Janke, D. J. Dirkes, S. Dovletgeldi, C. Liu, X. Qin, K. Gundogdu, W. You, V. Blum, and D. B. Mitzi, J. Am. Chem. Soc. **141**, 7955 (2019).
[32]B. A. Connor, L. Leppert, M. D. Smith, J. B. Neaton, and H. I. Karunadasa, J. Am. Chem. Soc. **140**, 5235 (2018).
[33]H.-J. Feng, W. Deng, K. Yang, J. Huang, and X. C. Zeng, J. Phys. Chem. C **121**, 4471 (2017).
[34]S. Zhao, K. Yamamoto, S. Iikubo, S. Hayase, and T. Ma, J. Phys. Chem. Solids **117**, 117 (2018).
[35]L. R. Morss, M. Siegal, L. Stenger, and N. Edelstein, Inorg. Chem. **9**, 1771 (1970).
[36]M. Shimizu, M. Koshimizu, Y. Fujimoto, T. Yanagida, S. Ono, and K. Asai, Opt. Mater. **61**, 115 (2016).
[37]P. Barbier, M. Drache, G. Mairesse, and J. Ravez, J. Solid State Chem. **42**, 130 (1982).
[38]M. Wang, P. Zeng, Z. Wang, and M. Liu, Adv. Sci. **7**, 1903662 (2020).
[39]J. D. Majher, M. B. Gray, T. A. Strom, and P. M. Woodward, Chem. Mater. **31**, 1738 (2019).
[40]M. M. Yao, L. Wang, J. S. Yao, K. H. Wang, C. Chen, B. S. Zhu, J. N. Yang, J. J. Wang, W. P. Xu, Q. Zhang, and H. B. Yao, Adv. Opt. Mater. **8**, 1901919 (2020).
[41]S. E. Creutz, E. N. Crites, M. C. De Siena, and D. R. Gamelin, Nano Lett. **18**, 1118 (2018).
[42]Y. Bekenstein, J. C. Dahl, J. Huang, W. T. Osowiecki, J. K. Swabeck, E. M. Chan, P. Yang, and A. P. Alivisatos, Nano Lett. **18**, 3502 (2018).
[43]P. M. Woodward, T. Vogt, D. E. Cox, A. Arulraj, C. N. R. Rao, P. Karen, and A. K. Cheetham, Chem. Mater. **10**, 3652 (1998).
[44]I. O. Troyanchuk, N. V. Kasper, D. D. Khalyavin, A. N. Chobot, G. M. Chobot, and H. Szymczak, J. Phys.: Condens. Matter **10**, 6381 (1998).
[45]J. Xu, J.-B. Liu, J. Wang, B.-X. Liu, and B. Huang, Adv. Funct. Mater. **28**, 1800332 (2018).
[46]C. Li, X. Lu, W. Ding, L. Feng, Y. Gao, and Z. Guo, Acta Crystallogr. **64**, 702 (2008).
[47]G. Volonakis, A. A. Haghighirad, R. L. Milot, W. H. Sio, M. R. Filip, B. Wenger, M. B. Johnston, L. M. Herz, H. J. Snaith, and F. Giustino, J. Phys. Chem. Lett. **8**, 772 (2017).
[48]P. E. Tomaszewski, Phase Transitions **38**, 127 (1992).
[49]M. R. Filip, S. Hillman, A. A. Haghighirad, H. J. Snaith, and F. Giustino, J. Phys. Chem. Lett. **7**, 2579 (2016).
[50]G. Volonakis, M. R. Filip, A. A. Haghighirad, N. Sakai, B. Wenger, H. J. Snaith, and F. Giustino, J. Phys. Chem. Lett. **7**, 1254 (2016).
[51]S. Radhakrishna and R. S. S. Setty, Phys. Rev. B **14**, 969 (1976).
[52]L. Wang, Q. Sun, Q. Liu, and J. Shi, J. Solid State Chem. **191**, 142 (2012).
[53]J. Xue, X. Wang, J. H. Jeong, and X. Yan, Phys. Chem. Chem. Phys. **20**, 11516 (2018).
[54]J. Wu, W. Walukiewicz, W. Shan, K. Yu, J. Ager III, E. Haller, H. Lu, and W. J. Schaff, Phys. Rev. B **66**, 201403 (2002).
[55]G. Henkelman, A. Arnaldsson, and H. Jónsson, Comput. Mater. Sci. **36**, 354 (2006).
[56]A. D. Becke and K. E. Edgecombe, J. Chem. Phys. **92**, 5397 (1990).
[57]A. Savin, R. Nesper, S. Wengert, and T. F. Fässler, Angew. Chem., Int. Ed. **36**, 1808 (1997).
[58]P. De Silva, J. Korchowiec, and T. A. Wesolowski, ChemPhysChem **13**, 3462 (2012).